Chapter 45
The Study on Fatigue Test of Cab With Suspension Based on 4-Channel Road Simulation Rig

Yunkai Gao, Genhai Wang and Jingpeng Han

Abstract In this chapter, the fatigue test method is studied based on 4-channel road simulation rig, which examine fatigue performance of truck cab with vehicle frame and suspension system. The motion of the cab is analyzed. The inner force of exciter and fixture is reduced through frame design and fixture design, and ADMAS is used to validate the method. Then the acceleration signal is regarded as the target signal, the load spectrum is reproduced in the test rig through physical iteration. Finally, the weakness of the cab obtained is similar to results of proving ground test.

Keywords 4-channel · Cab · Frame design · Test rig design · Road simulation test

45.1 Introduction

Vehicle body endures alternating load, the fracture failure of body frame is mainly caused by fatigue damage [1]. The fatigue resistance of the auto body can be examined accurately through fatigue test. There are three main types: road test, proving ground test and road simulation test. The road simulation test can cut down the testing period greatly, save manpower and the material resources, and be free effect in environment, season and weather comparing with two formers. Gao et al. [2], based on the loading spectrum collected in the road test, designed the bench test. And the design weaknesses were checked out. The remote parameter control technology was applied by Zhou [3] to obtain the loading spectrums for test in the test bench, and the dynamic strength test of car body structures in the test room was

Y. Gao · G. Wang (✉) · J. Han
Shanghai Key Lab of Vehicle Aerodynamics and Vehicle Thermal Management Systems, Shanghai, China
e-mail: wgenhai@163.com

Y. Gao · G. Wang · J. Han
School of Automotive Studies, Tongji University, Shanghai, China

Society of Automotive Engineers of China (SAE-China), *Proceedings of SAE-China Congress 2016: Selected Papers*, Lecture Notes in Electrical Engineering 418,
DOI 10.1007/978-981-10-3527-2_45

conducted. The laboratory road simulation test for truck cab was conducted by Gosavi [4], and the development cycle of semi-float truck cab was shortened. The road surface excitation reappearance experiment of a three-axle-heavy-duty truck was carried out with 6-channel road simulator by Jiang [5]. The compression and extrapolation of load spectrum of a heavy off-road vehicle collected from proving ground were conducted by Zhao [6] to obtain the target load spectrum used in bench simulation test.

Based on 4-channel road simulation rig, the cab with suspension is taken the research object in this chapter, the inner force of fixture and the actuator cylinder is decreased through frame processing and test rig design. Taking the acceleration signal as the target signal, the loading spectrum collected in the road test is reproduced in the test rig through physical iteration, and the design weaknesses of the cab are checked out. This paper has great engineering value for evaluating the heavy truck cab through road simulation test.

45.2 Acquisition and Processing of Road Load Spectrum

45.2.1 Acquisition of Road Load Spectrum

In this chapter, the acceleration signal measured at connection point of suspension on the cab is taken as target signal. Meanwhile, the suspension deflections and strain signal of mount point of rear suspension on cab longitudinal beam are measured. The signal acquisition sensors are shown in Table 45.1.

The test roads include beating road, bumpy road, long-wave road, short-wave road, cobblestones road, distortion road, fish-scale pits road, washboard road, Belgium road, sandstone road, pave road, off road and snake road.

45.2.2 Signal Analysis and Processing

To improve the authenticity and reliability of collected data, the signal should be processed. The signal processing usually comprises several parts: data editing and layout, trend component elimination, singular points elimination, stationarity and normality test, etc. The comparison of singular points elimination is shown in the Fig. 45.1.

Table 45.1 Sensors used for acquiring signals

Sensor	Number	Signal	Positional distribution
Accelerometer	12	Frame and cab acceleration	Frame side rail and cab longitudinal beam
Displacement sensor	4	Suspension deflections	Front and rear suspension
Strain gauge	2	Strain signal	Mount point of rear suspension

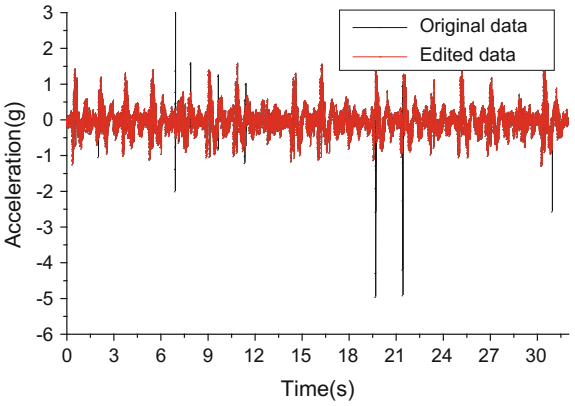

Fig. 45.1 The comparison of singular points elimination

Table 45.2 The amplitude statistic of acceleration signal

Channel	Minimum/g	Maximum/g	RMS/g	Average/g
LF acceleration	−2.25328	1.93766	0.467266	−0.006345
RF acceleration	−2.34484	2.19366	0.520277	0.008221
LR acceleration	−1.56177	1.45071	0.329362	0.05785
RR acceleration	−1.2883	1.50161	0.347018	0.050816

The statistics analysis in amplitude and frequency domain was conducted. The eigenvalue of amplitude includes minimum, maximum, root mean square value and average of the signal. The amplitude statistic of different roads shows that the acceleration in the front part of frame is larger than the rear part. The amplitude statistic of acceleration signal, measured at bumpy road, is shown in Table 45.2. The auto-power spectral density reflects the intensity of different frequency components. According to the auto-power spectral density of acceleration, the energy of acceleration signal concentrates in low frequency, which is lower than 30 Hz.

45.3 The Design of Test Rig

45.3.1 The Motion Analysis of Cab

The frame and cab was mounted on 4 actuator cylinders by 4 spherical hinges which was fixed on the cross beam of the frame. The cab has three degree of freedoms, namely vertical displacement Z, X-rotation Φ and Y-rotation Θ. The left front cylinder, right front cylinder, left rear cylinder and right rear cylinder are given number z_1, z_2, z_3, z_4 respectively. The distance between z_1 and z_2, or z_3 and z_4 is 750 mm, and between z_1 and z_3, or z_2 and z_4 is 1630 mm. The freedom synthesis matrix H can be derived from the geometrical relationship,

$$H = \begin{bmatrix} 0.25 & 0.25 & 0.25 & 0.25 \\ 0.667 & -0.667 & 0.667 & -0.667 \\ -0.307 & -0.307 & 0.307 & 0.307 \end{bmatrix}$$

and $DOF = H \cdot L$, $DOF = [Z \quad \Phi \quad \Theta]^T$, $L = [z_1 \quad z_2 \quad z_3 \quad z_4]^T$. The driving signal of actuator cylinder can be transformed into the motion of cab, and meanwhile the freedom decomposition matrix H^{-1} can be obtained,

$$H^{-1} = \begin{bmatrix} 1 & 0.375 & -0.815 \\ 1 & -0.375 & -0.815 \\ 1 & 0.375 & 0.815 \\ 1 & -0.375 & 0.815 \end{bmatrix}$$

and $L = H^{-1} \cdot DOF$, the motion of cab can be transformed into the driving signal of actuator cylinder by matrix H^{-1}.

45.3.2 Frame Design

The cab is installed on the frame through 4 suspensions. The long frame in actual vehicle can't be installed on the test rig directly, and the kinetics response of suspension system is mainly caused by the front part of frame. So the rear part of frame is cut off. The test rig is a typical redundant actuation mechanism with 4 vertical driving signals. When frame being twisted, the cylinders will be subjected to bending moment, which caused by lateral force. If the frame has large torsion stiffness, the cylinder and fixture would be damaged, and large stiffness will induce inter coupling between response signals. So the two large cross beams are replaced by two small cross beams.

45.3.3 Multi-Body Dynamics Simulation

ADMAS is used to analyze the dynamic response of different frame. In order to reflect the effect of frame stiffness to fixture, the modal neutral file is imported into ADMAS and the rigid frame is converted into flexible. The spherical hinges and fixtures are replaced by spherical pairs in ADMAS. Multi-body dynamic models are shown in Figs. 45.2 and 45.3.

4 sin-wave driving signals, whose amplitude is 15 mm, are applied to 4 actuator cylinders, and induce torsion deformation. And then the lateral forces of 4 spherical pairs are shown in Table 45.3. According to statistical results, the lateral forces of 4 spherical pairs which linked to 4 actuator cylinders, are induced significantly.

The statistic results of collected loading spectrum show that, the acceleration of front part of frame is bigger than rear part. The fixture and spherical hinge installed in front will endure bigger lateral force during the text. 2 spherical hinges are installed at

Fig. 45.2 Initial frame

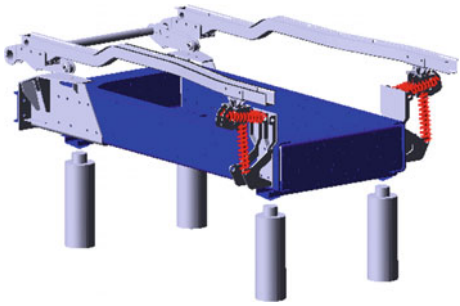

Fig. 45.3 Modified frame

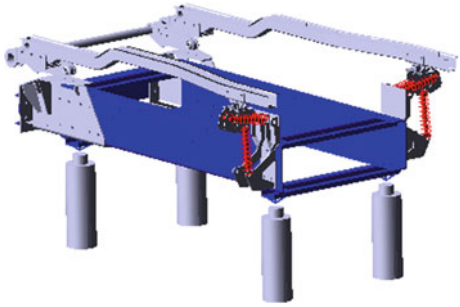

Table 45.3 Lateral forces of 4 spherical pairs

	Initial frame	Modified frame
LF spherical pair/N	97,154	34,767
RF spherical pair/N	97,273	30,652
LR spherical pair/N	91,269	21,780
RR spherical pair/N	96,185	24,621

Fig. 45.4 Lateral force of LF spherical pair

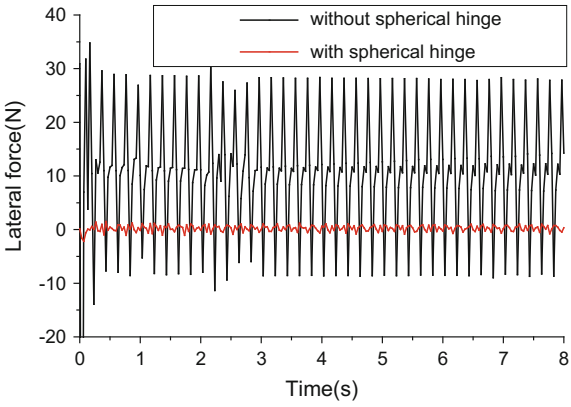

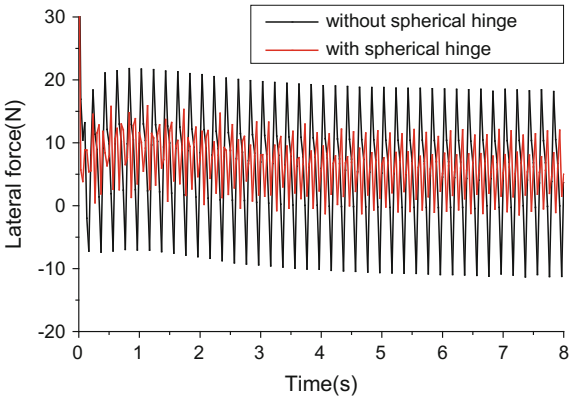

Fig. 45.5 Lateral force of LR spherical pair

the bottom of 2 front cylinders. And simulation is conducted in ADMAS. The comparison of lateral force is shown in Figs. 45.4 and 45.5.

Figures 45.4 and 45.5 show that spherical hinges installed at the bottom of 2 front cylinders can reduce the lateral force of spherical pairs significantly. Simulation results provide theoretical basis and reference for construction of test rig.

45.3.4 Construction of Test Rig

The cab and frame should be installed on test rig before physical iteration and durability test. The test rig can directly influence the accuracy of physical iteration and durability test. Fixtures are designed to link cab and frame to 4 actuator cylinders. 4 spherical hinges are fixed to mount point of leaf spring. The installation method is shown in Fig. 45.6. ADMAS simulation results show that spherical hinges installed at the bottom of 2 front cylinders can reduce the lateral force of spherical pairs significantly, and the installation is shown in Fig. 45.7.

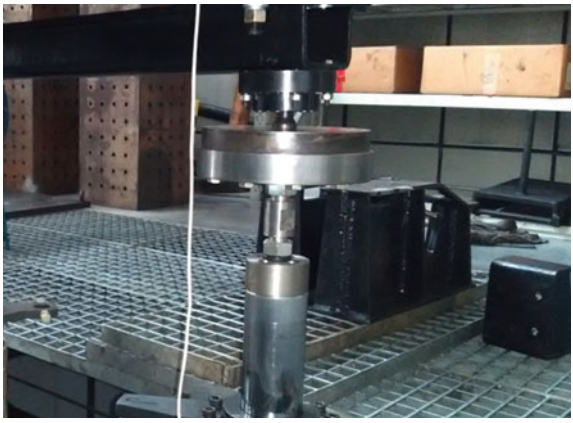

Fig. 45.6 Installation of fixtures

Fig. 45.7 Installation of spherical hinges

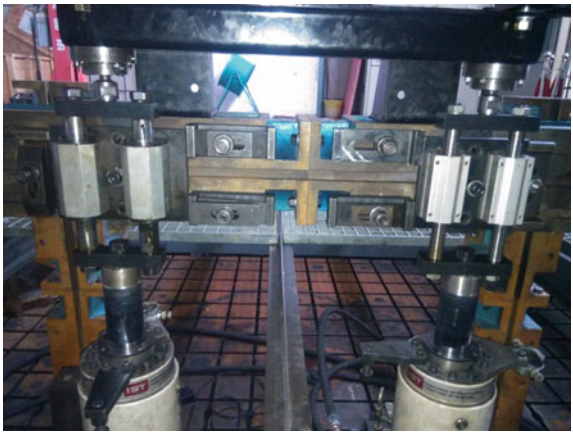

Fig. 45.8 Installation of linear guides

To prevent rear cylinders enduring excessive lateral forces, 2 linear guides are mounted on 2 rear cylinders, and the 2 guides are also fixed to a supporter. Screw connection should have enough pre-tightening force. The installation of linear guides is shown in Fig. 45.8, and the whole test rig is shown in Fig. 45.9.

45.4 Physical Iteration of Load Spectrum

The load spectrum is reproduced through physical iteration. Physical iteration consists of two steps, system identification and target signal iteration.

Fig. 45.9 Test rig

45.4.1 System Identification

The system, which is identified in this chapter, includes controller, electro—hydraulic servo control system, hydraulic cylinder, cab-suspension-frame assembly, acceleration sensors, fixtures, etc. Input signal of the whole system consist of 4 vertical displacements of cylinders. Response signal includes 4 acceleration signals from frame, and the location of acceleration sensors should be consistent with the location, where acceleration sensors located when collecting load spectrum. It is known that the energy of acceleration is concentrated below 30 Hz according to frequency domain analysis. Frequency response function is obtained by white pink noise, whose energy is concentrated below 35 Hz, driving cylinders. The quality of frequency response function is usually evaluated by coherence function. The closer to 1 coherence function is, the better frequency response function is. In engineering practice, the frequency response, whose coherence function is 0.8–0.9, is accurate and reliable.

45.4.2 Target Signal Iteration

The driving signals of cylinders can be obtained based on the frequency response function. Errors, caused by nonlinear system, should be eliminated by iteration. The major process is as follows [7].

When obtaining the first driving signal, a weighted coefficient $\alpha(0<\alpha<1)$ is introduced to prevent excessive signal and divergence of iteration.

$$U_1(f) = \alpha \cdot H^{-1}(f) \cdot T(f)$$

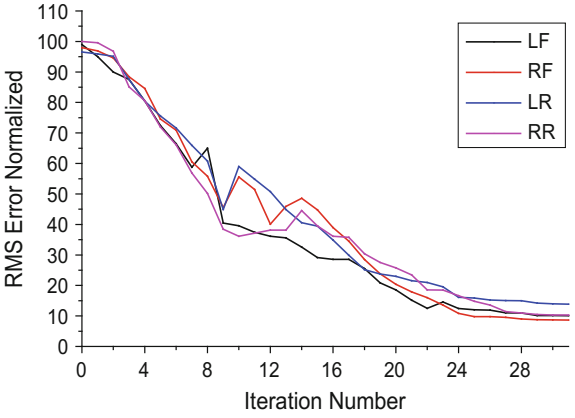

Fig. 45.10 RMS error plot for iteration

$U_1(f)$—Fourier transform of Initial driving signal $U_1(t)$; $H^{-1}(f)$—Inverse matrix of transfer function $H(f)$; $T(f)$—Fourier transform of target signal $T(t)$; α—weighted coefficient. Response signals of whole system are obtained by playing driving signals. The error $E(t) = T_n(t) - T(t)$ is also obtained ($T_n(t)$-Response signal of n times iteration), and driving signal of next iteration is revised according to the error.

$$\Delta U(f) = \beta \cdot H^{-1}(f) \cdot E(f)$$
$$U_{n+1}(f) = U_n(f) + \Delta U(f)$$

$\Delta U(f)$—Increment of driving signal; $E(f)$—Fourier transform of $E(t)$; β—weighted coefficient $(0 < \beta < 1)$; $U_{n+1}(f)$—Fourier transform of n + 1 times iteration; $U_n(f)$—Fourier transform of n times iteration. The quality of physical iteration is usually evaluated by relative mean square error between response signal and the target signal for the system whose target signal is acceleration.

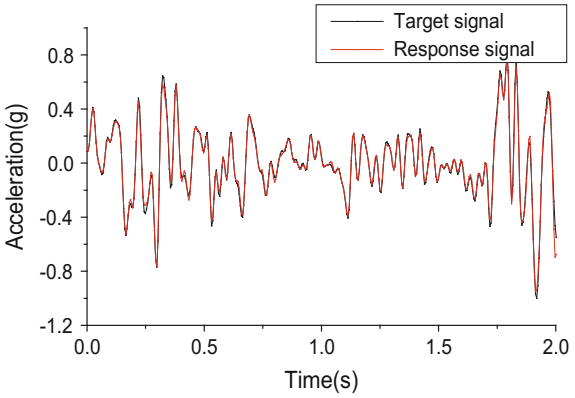

Fig. 45.11 Comparison in time domain

Table 45.4 The results of road simulation test and proving ground test (+: Yes, −: No)

Weak location	Road simulation test	Proving ground test
The lower side of the solder joint of front cab	+	+
The weld between outer panel front wall and engine cabin	+	+
The weld between front wall and engine cabin	+	+
Roundness of front wall	+	−
The weld between front stringer and floor	+	+
The corner floor stringer	+	+
The door cannot be completely closed	+	+
The bolts of the cab tilting mechanism loose	+	+
The weld around the lower part of the front cabin	+	+
The crack of cabin dashboard	+	+

$$\varepsilon = \frac{RMS(E(t))}{RMS(T(t))}$$

ε—Relative mean square error; $RMS(\cdot)$—Root mean square. Generally speaking, iteration can be stopped as long as $\varepsilon \leq 10\%$. RMS error plot for iteration is shown in Fig. 45.10. The iterative signals and the target signals have a highly consistency in time domain and as shown in Fig. 45.11.

45.5 Test and Result

The driving signal from the last iteration is arranged in accordance with the road load spectrum acquisition sequence. Then the driving signal is played again and again until the test is completed. Finally, the result of road simulation test is consistent with the proving ground test. The test results are shown in Table 45.4 and the weld crack between front wall and engine cabin is shown in Fig. 45.12.

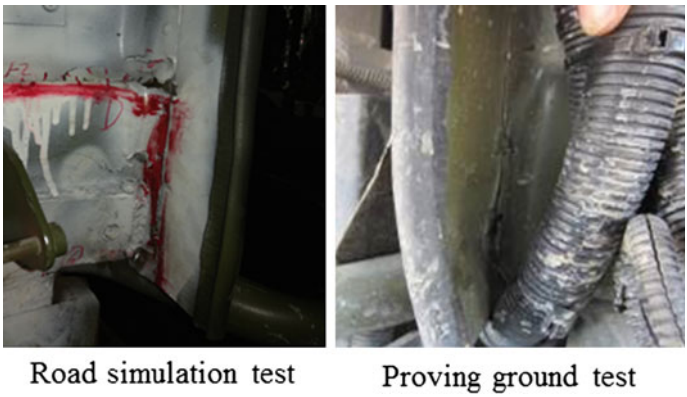

Fig. 45.12 The weld crack between front wall and engine cabin

45.6 Conclusion

Based on the 4-channel road simulator test rig, the fatigue durability performance of the truck cab with vehicle frame and suspension system is checked out. The result of road simulation test is consistent with proving ground test. This test is also a successful further use of 4-channel road simulation rig, and the purpose, small test rig loading a large load, is achieved. This paper has great engineering value for evaluating the heavy truck cab through road simulation test.

References

1. Gao Y (2006) Structural analysis of vehicle body. Beijing Institute of Technology Press, Beijing
2. Gao Y, Fang J, Xie M (2012) Durability analysis and evaluation of a frame-type heavy truck cab. J Tongji Uni (Natural Sci) 40(5):723–728
3. Zhou H, Feng Z (2001) The application of remote parameter control technology in dynamic strength test of car body structures. Automobile Technol 2:20–22
4. Gosavi SS (2006) In lab truck cab and cab suspension durability validation. SAE Technical Paper
5. Jiang H, Dai Y, Lintao Y (2008) Road surface excitation reappearance experiment on heavy-duty truck based on 6-channel road simulator. Automobile Technol 9:46–49
6. Zhao X, Zhang Q, Jiang D (2009) The compression and extrapolation of load spectrum for a heavy off-road vehicle obtained from proving ground testing. Automotive Eng 31(9):871–875
7. Yudong H, Zhou H, Gang X (2012) Control algorithm of test rig for vehicle road simulation. J Tongji Uni (Natural Sci) 40(8):1244–1248